Photoelectron Imaging and Theoretical Studies of Silver Monohalides AgX− (X = Cl, Br, I) and AuCl−

ARTICLE *in* THE JOURNAL OF PHYSICAL CHEMISTRY A · JUNE 2011

Impact Factor: 2.69 · DOI: 10.1021/jp1100686 · Source: PubMed

6 AUTHORS, INCLUDING:

Hua Xie
Chinese Academy of Sciences
27 PUBLICATIONS **110** CITATIONS
SEE PROFILE

Kai Tan
Xiamen University
69 PUBLICATIONS **1,416** CITATIONS
SEE PROFILE

Zichao Tang
Chinese Academy of Sciences
66 PUBLICATIONS **517** CITATIONS
SEE PROFILE

Xin Lu
Xiamen University
100 PUBLICATIONS **3,107** CITATIONS
SEE PROFILE

THE JOURNAL OF PHYSICAL CHEMISTRY A

ARTICLE

pubs.acs.org/JPCA

Photoelectron Imaging and Theoretical Studies of Silver Monohalides AgX^- (X = Cl, Br, I) and $AuCl^-$

Xia Wu,[†] Hua Xie,[†] Zhengbo Qin,[†] Kai Tan,[‡] Zichao Tang,*[,†] and Xin Lu*[,‡]

[†]State Key Laboratory of Molecular Reaction Dynamics, Dalian Institute of Chemical Physics, Chinese Academy of Sciences, Dalian 116023, China

[‡]State Key Laboratory of Physical Chemistry of Solid Surface & Fujian Provincial Key Laboratory of Theoretical and Computational Chemistry, Department of Chemistry, College of Chemistry and Chemical Engineering, Xiamen University, Xiamen 361005, China

Supporting Information

ABSTRACT: Photodetachment of AgX^- (X = Cl, Br, I) and $AuCl^-$ is studied by a photoelectron velocity map imaging technique and theoretical calculations. Photoelectron spectra (PES) and photoelectron angular distributions (PADs) were obtained. The vibrationally resolved spectra provided approximately equal electron affinities (EAs) for AgX: 1.593(22) eV for AgCl, 1.623(21) eV for AgBr, and 1.603(22) eV for AgI, respectively. Franck−Condon simulations of these spectra gave the equilibrium bond lengths and vibrational frequencies of the title anions. Relativistic density functional theory (DFT) calculations using BLYP, PW91, PBE, and BP86 functionals have been performed to predict the EAs of the AgX (X = Cl, Br, I) molecules. The computed EAs at the BP86 level of theory are in good agreement with the experimental values. Energy partitioning analyses (EPA) at the BP86(ZORA)/QZ4P level of theory of both anions and their neutrals were reported.

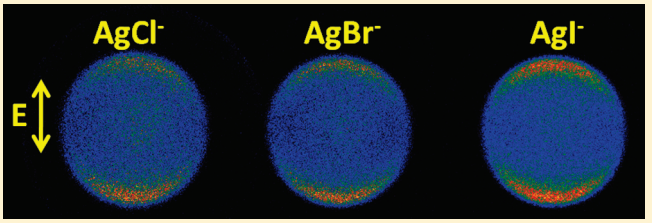

1. INTRODUCTION

Silver halides have been of interest due to their important role in photography and holography, and each silver monohalide has been regarded as a paradigm for a chemical bond involving a transition metal atom. Experimentally, silver chloride and silver bromide have been studied extensively. Several rational experiments were carried out to measure the equilibrium bond lengths and the vibrational frequencies of the neutral AgCl,[1,2] AgBr,[3] and AgI.[4] Photoionization photoelectron spectra of AgCl, AgBr, and AgI vapor were also reported.[5] Theoretically, there has been a wealth of benchmark effort for the computations of AgX (X = Cl, Br, I) molecules,[6,7] mainly focusing on their geometric parameters and vibrational frequencies. For example, the CCSD(T) calculations on the molecular structures of AgX (X = Cl, Br, I)[7] turn out to well reproduce the experimental data. In contrast to the neutral AgX, such information of anionic AgX^- as equilibrium bond lengths and ground-state harmonic frequencies is yet unavailable.

Electron affinity (EA) is one of the important molecular properties, which is often measured by the amount of energy required to detach an electron from a singly charged anion of a molecule (anion photoelectron spectroscopy).[8] Some relevant experiments were carried out by using anion photoelectron spectroscopy to measure the EAs of CuX_2 (X = Cl, Br)[9] and AuX_2 (X = Cl, Br, I),[10] but there is no report of the EAs of AgX (X = Cl, Br, I). It is interesting that the EAs of $CuCl_2$ and $CuBr_2$ were found to be nearly identical, 4.35(5) eV.[9] On the contrary, the EAs of $AuCl_2$, $AuBr_2$, and AuI_2 were measured to be 4.60(7), 4.46(7), and 4.18(7) eV,[10] which are by ∼1.1 eV parallel higher than the atomic EAs of Cl (3.613 eV), Br (3.364 eV), and I (3.059 eV), respectively.[11] Despite the fact that the chemistry of gold is known to be remarkably different from its lighter congeners due to the strong relativistic effects,[12] the aforementioned experimental observations raise puzzling questions for copper halides and silver halides. For example, why do the lighter CuX_2 (X = Cl, Br) molecules with different halogen atoms have similar values of EA? Do silver halides, AgX_2 or AgX, show similar EA behavior?

Motivated by these questions, we performed photoelectron velocity map imaging and DFT calculations on silver monohalides as well as AuCl as a reference. The equilibrium bond lengths, harmonic frequencies, and the EA values of anionic AgX^- are reported for the first time. Moreover, relativistic density functional theory (DFT) calculations have been performed to benchmark the EAs of the AgX (X = Cl, Br, I) molecules using different density functions including BLYP, PW91, PBE, and BP86. The energy partitioning analyses (EPA) at the BP86(ZORA)/QZ4P level of theory of both anions and their neutrals are also discussed.

2. EXPERIMENTAL DETAILS

The experiments were carried out using an anion photoelectron velocity map imaging analyzer. The apparatus has been

Received: October 20, 2010
Revised: April 18, 2011
Published: May 26, 2011

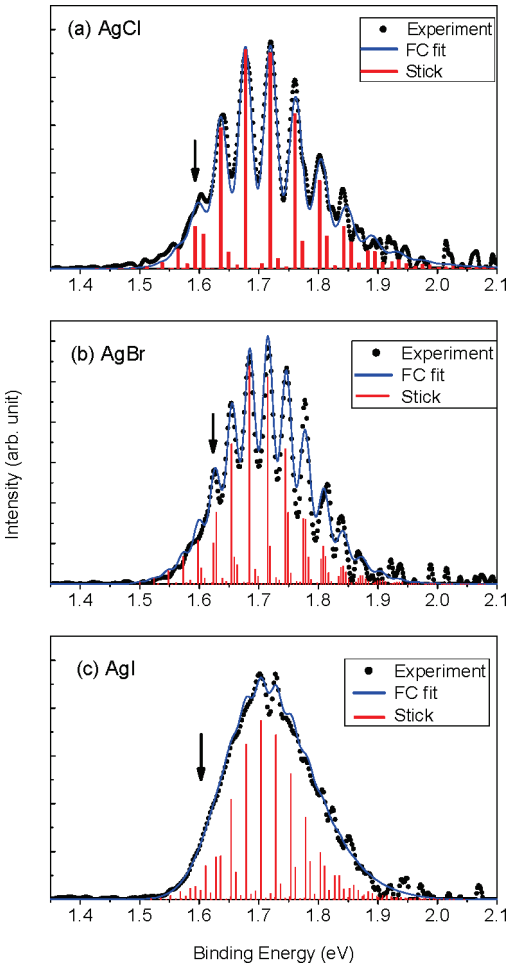

Figure 1. The 532 nm photoelectron spectra of AgX^- (X = Cl, Br, I). The black dots are experimental data and the red sticks and blue curves are from FC (Franck−Condon) simulations. The arrows indicate the adiabatic electron affinities (EAs).

described in detail elsewhere.[13] Briefly, anions were generated by a laser vaporization source. Silver monohalide anions $AgBr^-$ and AgI^- were produced by laser vaporization of a silver bromide (99%) or silver iodide (99%) target in the presence of pure helium gas. Anions $AgCl^-$ and $AuCl^-$ were generated by laser vaporization of the pure silver or gold target (99.9%), and helium (99.9%) gas was seeded with a small amount of carbon tetrachloride (CCl_4, analytically pure) molecules.

In the imaging experiments, the AgX^- anions crossed with the 532 nm photons of a Nd:YAG laser for photodetaching excess electrons. For $AuCl^-$, the 450 nm detachment photons of a dye laser were used. The laser propagates perpendicularly to the anion beam axis, with a polarization vector parallel to the surface of the imaging detector. The photoelectrons were pushed onto an imaging detector by collinear velocity map imaging (VMI) electrodes.[14] The imaging detector consisted of a 40 mm diameter microchannel plate (MCP) assembly, phosphor screen, and a CCD camera. All the photoelectron images were reconstructed using the BASEX program,[15] which yielded both the photoelectron kinetic energy spectra and anisotropy parameters. The photoelectron kinetic energy spectra were calibrated by the known spectrum of Au^-. The photoelectron spectra (PES) were plotted against electron binding energy (eBE) = $h\nu$ − eKE,

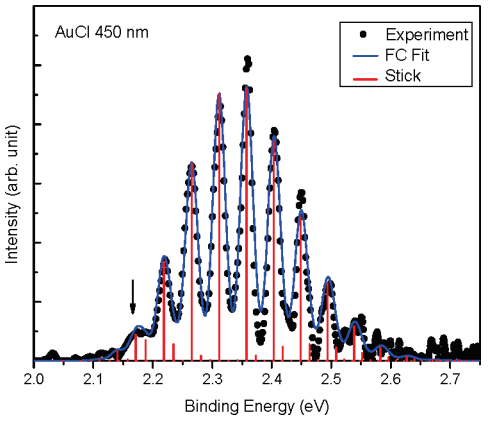

Figure 2. The 450 nm photoelectron spectrum of $AuCl^-$. The black dots are experimental data and the red sticks and blue curves are from FC (Franck−Condon) simulations. The black arrow indicates the adiabatic electron affinity (EA).

where $h\nu$ is the photon energy. The energy resolution was about 30 meV full width at half-maximum (fwhm) at electron kinetic energy (eKE) of 1 eV.

3. COMPUTATIONAL DETAILS

Density functional theory (DFT) calculations were performed to elucidate the geometric and electronic structures of the anionic and neutral AuCl and AgX (X = Cl, Br, I) species. We have employed several density functions, including BLYP,[16] PW91,[17] PBE,[18] and BP86[16a,19] as implemented in the ADF2007.01 program.[20] The standard basis sets ZORA/QZ4P were used for Au, Ag, Cl, Br, and I, with the small frozen-core approximation. The scalar relativistic effects and spin−orbital coupling effects were taken into account by using the ZORA (zero order regular approximation) and SP-ZORA formalisms, respectively.[21] Analytical frequency calculations were performed at the BP86-(ZORA)/QZ4P level of theory.

The nature of chemical bonding within the title complexes was obtained by means of the energy partitioning analysis (EPA) method.[22] The total interaction energy ΔE_{int} corresponds to the energy change when the constituting fragments are combined to form the overall molecule. It can be decomposed into three physically meaningful parts

$$\Delta E_{int} = \Delta E_{elstat} + \Delta E_{Pauli} + \Delta E_{orb} \quad (1)$$

ΔE_{Pauli} denotes the Pauli repulsion energy between the fragments. ΔE_{elstat} is the electrostatic interaction energy between the fragments with unrelaxed electron densities. ΔE_{orb} is the orbital interaction energy between the fragments due to the relaxation of Kohn−Sham orbitals in the SCF procedure. The orbital interaction energy ΔE_{orb} can be further decomposed into the contributions from each irreducible representation of the interacting system, e.g., σ-orbital and π-orbital interactions in the MX molecules concerned. For neutral MX molecules, two different schemes of fragmentation were adopted, i.e., the homolytic scheme using M and X atomic fragments and the heterolytic scheme using M^+ and X^- ionic fragments. For anionic MX^-, the fragments are M^0 and X^-. All EPA analyses were performed at the BP86 (ZORA)/QZ4P level of theory.

For comparison, high-level CCSD(T) calculations[23] were performed to obtain the structures and EAs of AgX (X = Cl, Br, I)

Table 1. Spectroscopic and Geometric Parameters[a] of $AgX^{0/-}$ (X = Cl, Br, I) and $AuCl^{0/-}$

		Ag−X (Å)		frequency (cm^{-1})		
species		neutral	anion	neutral	anion	EA (eV)
AgCl	expt	2.280[b]	2.436(10)	344[b]	245(20)	1.593(22)
	calcd[c]	2.288	2.472	329	211	1.566
AgBr	expt	2.393[b]	2.529(10)	248[b]	212(20)	1.623(21)
	calcd[c]	2.410	2.612	238	148	1.581
AgI	expt	2.545[b]	2.720(10)	206[b]	141(30)	1.603(22)
	calcd[c]	2.574	2.789	194	118	1.577
AuCl	expt	2.200[d]	2.354(10)	384[d]	210(20)	2.217(12)
	calcd[c]	2.216	2.432	334	211	2.092

[a] The error bars for the optimized parameters represent a 95% confidence level. [b] Experimental data extracted from ref 4. [c] BP86(SP-ZORA)/QZ4P-prediction with ZPE-corrections. [d] Experimental data extracted from ref 27.

molecules using Gaussian 03.[24] The all-electron 6-311+G(3df) basis set was used for chlorine. For Br, I, and Ag, the Stuttgart quasi-relativistic effective core potentials (ECPs) were used, i.e., 28-electron−core ECPs for Ag and Br and 46-electron−core ECPs for I, in combination with basis sets (14s10p3d2f1g)/[4s4p3d2f1g] for Br and I and (8s7p6d2f1g)/[6s5p3d2f1g] for Ag.[25] Such a combination of basis sets is denoted "LB". Noteworthily, previous CCSD(T)/LB calculations by Hargittai et al. gave accurate predictions on the geometric parameters and vibrational frequencies of AgX (X = F, Cl, Br, I) molecules.[7]

4. RESULTS AND DISCUSSION

4.1. Photoelectron Imaging. Figure 1 shows the photoelectron spectra of $AgCl^-$, $AgBr^-$, and AgI^- obtained at 532 nm (2.331 eV). The 450 nm (2.755 eV) photoelectron spectrum of $AuCl^-$ is displayed in Figure 2. Due to the low photon energies, each of these spectra exhibits only one vibrationally resolved spectral band from the electronic ground state of particular anion to that of the corresponding neutral electronic ground state. In addition, the spectra of $AgCl^-$ and $AgBr^-$ show better resolved vibrational peaks than that of AgI^-, as the former two anions have higher frequencies of Ag−X stretching. The positions of the arrows (Figures 1 and 2) indicate the adiabatic electron affinities (EAs), determined from the 0−0 vibrational transition. The weak peaks below the EA values are vibrational hotbands, which are from the anion vibrational excitation states to the ground vibrational level of the neutral species.

To confirm the peak assignments and gain more spectroscopic parameters, Franck−Condon (FC) simulations were performed using the PESCAL program.[26] The electronic ground states of the anions and neutral species were modeled as Morse oscillators. From FC simulations, the vibrational frequencies, EAs, and the differences of the bond lengths between the neutral and anionic species can be obtained. As the parameters of the neutral (r_e, w_e, w_ex_e) species were known and fixed (see Table 1),[4,27] we can get the bond lengths of the anionic species. The simulated spectra are also plotted in Figures 1 and 2 as blue curves. Molecular constants and EA values derived from the transition assignments and the FC simulations are summarized in Table 1, serving as experimental data. For each of the MX molecules concerned, FC simulations show a longer M−X bond length for the ground state

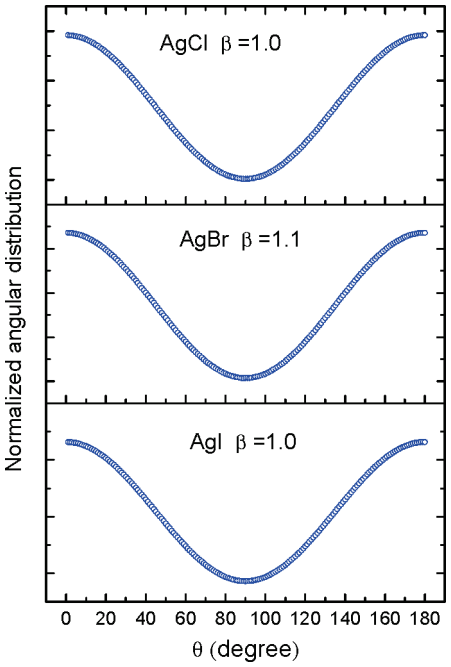

Figure 3. The photoelectron angular distributions of AgX^- (X = Cl, Br, I) at 532 nm.

of the anion than that of the neutral species. The as-determined $r_e(AgX^-) - r_e(AgX)$ for X = Cl, Br, I are 0.156, 0.136, and 0.175 Å, respectively, in line with the lower vibrational frequencies of the anions compared to the neutral species. The equilibrium bond lengths of the anionic and neutral $AuCl^{-/0}$ are also shorter than those of $AgCl^{-/0}$, likely due to relativistic bond contraction.

Figure 3 depicts the photoelectron angular distributions (PADs) of $AgCl^-$, $AgBr^-$, and AgI^-. The anisotropy parameter (β) can be obtained by fitting the function[28]

$$I(\theta) \propto 1 + \beta P_2(\cos\theta) \qquad (2)$$

to the angular distributions derived from the reconstructed images. The anisotropy parameters (β) were between −1 and +2, corresponding to perfectly perpendicular and perfectly parallel transitions, respectively. The measured anisotropy parameters (β) of AgX^- (X = Cl, Br, I) and $AuCl^-$ are 1.0, 1.1, 1.0, and 1.38, respectively. All of the ground-state transitions are parallel transitions. Interestingly, the PAD behaviors for AgX (X = Cl, Br, I) are similar.

From Figure 1, the measured EAs of AgCl (1.593(22) eV), AgBr (1.623(21) eV), and AgI (1.603(22) eV) are remarkably similar, in sharp contrast to the difference in the atomic EAs: Cl ∼ 3.613 eV, Br ∼ 3.364 eV, and I∼3.059 eV.[11] If the chemical bonding in both the AgX and AgX^- (X = Cl, Br, I) species is mainly ionic, their EAs should be mainly determined by the electron affinity of the Ag cation and the electrostatic interaction energy between cation and halide anion. It can be estimated that the electrostatic attraction energy between Ag^+ and X^- decreases from Cl to I upon increasing Ag^+−X^- distance. Thus the invariance in the EAs of AgX molecules suggests that the covalence of the Ag−X bonding increases from AgCl to AgI. The measured EA of AuCl is 2.217 eV, by ∼0.5 eV higher than that of AgCl, due to the higher electronegativity of Au than that of the Ag atom.

Table 2. DFT-Computed Electron Affinities (EA, in eV) for AgX (X = Cl, Br, I) Molecules Using Different Density Functions and (ZORA)/QZ4P Basis Sets and the CCSD(T)/LB-Predicted Data

	BLYP	PW91	PBE	BP86	CCSD(T)
AgCl	1.485	1.467	1.422	1.557	1.499
AgBr	1.495	1.482	1.437	1.575	1.435
AgI	1.491	1.491	1.446	1.583	1.472
MSE[a]	−0.116	−0.126	−0.171	−0.035	−0.137

[a] Mean signed error.

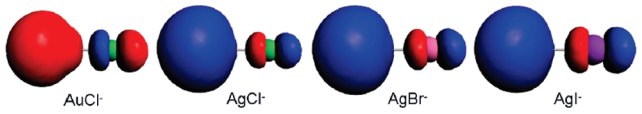

Figure 4. Singly occupied molecular orbital (isodensity value = 0.03) of $AuCl^-$ and AgX^- (X = Cl, Br, I).

4.2. Electron Affinities from Theoretical Calculations. Our CCSD(T)/LB calculations (Table S1 in the Supporting Information) reproduced the experimental geometry and vibrational frequency of AgX (X = Cl, Br, I), in agreement with previous theoretical work.[7] However, the CCSD(T)-computed EA values (Table 1) are lower than the experimental EA, by 0.094, 0.188, and 0.131 eV for X = AgCl, AgBr, AgI, respectively. Hence, we performed more benchmark calculations on the anionic and neutral AgX (X = Cl, Br, I) species using different density functions (BLYP, PW91, PBE, and BP86) with inclusion of scalar relativistic effects (ZORA) and the QZ4P basis sets. The DFT-predicted Ag−X bond lengths are listed in Table S2, Supporting Information. All the investigated density functions overestimate the Ag−X bond length for both anionic and neutral AgX species with the mean signed error (MSE) ranging from 0.035 to 0.092 Å. For each density functional method concerned, the MSE value derived from the anionic series is higher than that from the neutral series. Specifically, the BLYP functional performs the worst for predicting the Ag−X bond length, giving the largest MSE value of 0.092 Å. The other ones (PW91, PBE, BP86) perform much better, giving MSE values smaller than 0.04 Å. Accordingly, the predicted Ag−X bond lengths by these density functional methods are acceptable.

The DFT-computed EAs of AgX (X = Cl, Br, I) molecules are listed in Table 2. Briefly, all the investigated density functions underestimate the EAs of AgX (X = Cl, Br, I) molecules with MSE ranging from −0.035 (BP86) to −0.171 (PBE) eV. Among them, the PBE functional performs the worst, and the BP86 functional gives the best performance for calculating the EA of AgX molecules. Thus, among all investigated density functional methods, the BP86 functional performs the best for predicting both the geometries and EAs of AgX molecules.

We further investigate the relativistic effects on the BP86/QZ4P-predicted EAs of AgX (X = Cl, Br, I) and AuCl molecules by using ZORA and SP-ZORA formalisms. Table S3 (see Supporting Information) lists the BP86/QZ4P-predicted EAs along with the experimental values. The nonrelativistic BP86/QZ4P calculations severely underestimate the EA values, by 0.18 eV for the lightest AgCl molecule and by 0.67 eV for the heaviest AuCl molecule. Such underestimations become much smaller upon inclusion of scalar relativistic effects (ZORA); the BP86(ZORA)/QZ4P-computed EAs deviate from the experimental ones by only 0.04 eV for AgX molecules and 0.13 eV for AuCl. Further inclusion of the spin−orbital coupling effects (SP-ZORA) does not significantly improve the DFT predictions of EA values. Table 1 presents the M−X bond lengths, and the corresponding EA values of AgX (X = Cl, Br, I) and AuCl species computed at the BP86(SP-ZORA)/QZ4P level of theory. In summary, the relativistic effects using ZORA formalism for AgX molecules are rational and effective.

Table 3. Energy Decomposition (in kcal/mol) for the AgX^- (X = Cl, Br, I) and $AuCl^-$ Species with Fragments ($M^0 + X^-$)

	$AgCl^-$	$AgBr^-$	AgI^-	$AuCl^-$
ΔE_{int}	−27.1	−25.3	−23.3	−35.0
ΔE_{Pauli}	102.2	99.1	100.8	132.4
ΔE_{elstat}	−76.4	−74.3	−73.9	−96.9
ΔE_{orb}	−52.9	−50.1	−50.2	−70.5
ΔE_{σ}	−49.0	−46.6	−47.0	−65.3
ΔE_{π}	−3.9	−3.5	−3.2	−4.9

Table 4. Energy Decomposition (in kcal/mol) for the AgX (X = Cl, Br, I) and AuCl Molecules with Heterolytic Fragments ($M^+ + X^-$)

	AgCl	AgBr	AgI	AuCl
ΔE_{int}	−173.2	−171.0	−168.8	−207.6
ΔE_{Pauli}	98.5	92.9	88.4	159.7
ΔE_{elstat}	−214.8	−205.2	−194.2	−268.6
ΔE_{orb}	−56.9	−58.6	−63.0	−98.6
ΔE_{σ}	−41.6	−44.0	−48.2	−78.5
ΔE_{π}	−14.5	−13.8	−14.0	−18.9

4.3. Bonding Analysis. The lowest unoccupied molecular orbital (LUMO) of AgX molecule is mainly contributed by the valence 5s(Ag) atomic orbital with minor contribution from valence p_z orbitals of X atom. This orbital becomes singly occupied in AgX^-, i.e., SOMO of AgX^- species (Figure 4). The SOMO of $AuCl^-$ is similar, dominated by a 6s orbital of Au with non-negligible contribution from $3p_z$ atomic orbital of Cl. Thus AgX^- and $AuCl^-$ can be qualitatively described as a combination of two fragments $M^0 + Cl^-$.

Table 3 presents the data of EPA analyses on the AgX^- and $AuCl^-$ species. The ΔE_{elstat} term in all MX^- species is by ∼24 kcal/mol larger than the ΔE_{orb} term, suggesting the M^0-X^- bonding in these species is much more electrostatic than covalent. Further decomposition of the ΔE_{orb} term into the ΔE_{σ} and ΔE_{π} terms shows that the minor covalence of the M^0-X^- bonding arises dominantly from σ-orbital interactions with marginal contribution from π-orbital interactions. Among the four MX^- complexes concerned, the $AuCl^-$ has the largest value of ΔE_{orb}, indicating the covalence of $Au-Cl^-$ bonding is stronger than that of $Ag-X^-$ bonding. Surprisingly, the ΔE_{orb} term is nearly identical in both $AgBr^-$ and AgI^-, but slightly smaller than that in $AgCl^-$. It means the covalence of $Ag-X^-$ bonding is nearly identical in $AgBr^-$ and AgI^- complexes but marginally stronger in $AgCl^-$. Furthermore, the total interaction energy ΔE_{int} decreases gradually from $AgCl^-$ (−27.1 kcal/mol) to AgI^- (−23.3 kcal/mol), indicating the $Ag-X^-$ bonding is weakened from $AgCl^-$ to AgI^-. In addition, the $Au-X^-$ bonding with a

dx.doi.org/10.1021/jp1100686 |J. Phys. Chem. A 2011, 115, 6321–6326

ΔE_{int} value of −35.0 kcal/mol is stronger than the Ag−X^- bonding.

Table 4 presents the data from EPA analyses on the neutral AgX and AuCl molecules with use of heterolytic fragments ($M^+ + X^-$). We have also performed EPA calculations by using homolytic fragments ($M^0 + X^0$). However, for each molecule concerned, the ΔE_{orb} term derived from heterolytic fragments is much smaller than that derived from homolytic fragments (See Table S4 in the Supporting Information for details). This means the wave functions of MX molecules are more close to that consisting of heterolytic fragments than to that composed of homolytic fragments.[29] As such, the M−X bonding in MX molecules should be better described as M^+−X^- bonding, and the EPA calculations based on heterolytic fragments are employed for understanding of the chemical bonding in MX molecules.

As shown in Table 4, the ΔE_{elstat} term in all the MX molecules is 2−3 times larger than the ΔE_{orb} term, showing the M−-X bonding in all MX molecules is mainly ionic in nature. This again justifies the choice of heterolytic fragments ($M^+ + X^-$) for EPA calculations of the MX molecules. The ΔE_{orb} term gradually increases from −56.9 kcal/mol (AgCl) to −63.0 kcal/mol (AgI), showing the minor covalence in Ag^+−X^- bonding becomes stronger from AgCl to AgI. Due to relativistic effects,[30] the covalence of Au^+−Cl^- bonding turns to be the strongest, having a ΔE_{orb} value of −98.6 kcal/mol. Similar to the M^0−X^- cases, the covalence of M^+-X^- bonding arises mainly from σ-orbital interactions with ΔE_σ values ranging from −41.6 kcal/mol for AgCl to −78.5 kcal/mol for AuCl. However, the contribution of π-orbital interactions is non-negligible in the M^+−X^- cases (ΔE_π around 16 kcal/mol) but negligible in the M^0−X^- cases (ΔE_π < 5 kcal/mol).

Though the covalence of Ag^+−X^- bonding increases from AgCl to AgI, the electrostatic interaction energy (ΔE_{elstat}) decreases from −214.8 (AgCl) to −194.2 (AgI) kcal/mol upon increasing Ag^+−X^- bond length. As a whole, the total interaction of the Ag^+−X^- bonding gradually decreases from −173.2 (AgCl) to −168.8 (AgI) kcal/mol.

5. CONCLUDING REMARKS

We reported a combined photoelectron velocity map imaging and DFT investigation on the photodetachment of AgX^- (X = Cl, Br, I) and $AuCl^-$. The vibrationally resolved photoelectron spectra yield accurate electron affinities (EAs), 2.217(12) eV for AuCl, and nearly equal EA(AgX), 1.593(22) eV for AgCl, 1.623(21) eV for AgBr, 1.603(22) eV for AgI, respectively. Franck−Condon simulations give the accurate bond lengths and frequencies of the anion AgX^- and $AuCl^-$. Relativistic density functional calculations were carried out to compute the EAs of AgX molecules using different functionals including BLYP, PW91, PBE, and BP86. The BP86 functional performs the best in reproducing the experimental EA values. Energy partitioning analyses (EPA) disclose that the Ag−X bonding in either AgX^- or AgX species is much more ionic than covalent, and the minor covalence of Ag−X bonding increases from AgCl to AgI.

■ ASSOCIATED CONTENT

Supporting Information. Tables S1−S4 providing Ag−X bond lengths, computed EA values, and energy decomposition. This material is available free of charge via the Internet at http://pubs.acs.org.

■ AUTHOR INFORMATION

Corresponding Author

*E-mail: zctang@dicp.ac.cn (Z.C.T.); xinlu@xmu.edu.cn (X.L.).

■ ACKNOWLEDGMENT

This work is supported by the National Natural Science Foundation of China (Grant Nos. 20773126, 20973137), the Ministry of Science and Technology of China, and the Chinese Academy of Sciences.

■ REFERENCES

(1) Krisher, L. C.; Norris, W. G. *J. Chem. Phys.* **1966**, *44*, 391–394.
(2) Pearson, E.; Gordy, W. *Phys. Rev.* **1966**, *152*, 42–46.
(3) Krisher, L. C.; Norris, W. G. *J. Chem. Phys.* **1966**, *44*, 974–976.
(4) Herzberg, G. *Molecular Spectra and Molecular Structure, Constants of Diatomic Molecules IV. Constants of Diatomic Molecules*; Van Nostrand: New York, 1979.
(5) Berkowitz, J.; Batson, C. H.; Goodman, G. L. *J. Chem. Phys.* **1980**, *72*, 5829–5837.
(6) (a) Ramirez-Solis, A. *J. Chem. Phys.* **2002**, *117*, 1047–1054. (b) Amaro-Estrada, J. I.; Ramirez-Solis, A. *J. Chem. Phys.* **2009**, *131*, 124308–124309.
(7) Müller-Rösing, H.-C.; Schulz, A.; Hargittai, M. *J. Am. Chem. Soc.* **2005**, *127*, 8133–8145.
(8) (a) Ho, J.; Ervin, K. M.; Lineberger, W. C. *J. Chem. Phys.* **1990**, *93*, 6987–7002. (b) Peppernick, S. J.; Gunaratne, K. D. D.; Sayres, S. G.; Castleman, A. W. *J. Chem. Phys.* **2010**, *132*, 044302–044313. (c) Neumark, D. M. *J. Phys. Chem. A* **2008**, *112*, 13287–13301. (d) Bartels, C.; Hock, C.; Huwer, J.; Kuhnen, R.; Schwobel, J.; von Issendorff, B. *Science* **2009**, *323*, 1323–1327. (e) Sanov, A.; Mabbs, R. *Int. Rev. Phys. Chem.* **2008**, *27*, 53–85.
(9) Wang, X.-B.; Wang, L.-S.; Brown, R.; Schwerdtfeger, P.; Schroder, D.; Schwarz, H. *J. Chem. Phys.* **2001**, *114*, 7388–7395.
(10) Schroder, D.; Brown, R.; Schwerdtfeger, P.; Wang, X.-B.; Yang, X.; Wang, L.-S.; Schwarz, H. *Angew. Chem., Int. Ed.* **2003**, *42*, 311–314.
(11) Rienstra-Kiracofe, J. C.; Tschumper, G. S.; Schaefer, H. F.; Nandi, S.; Ellison, G. B. *Chem. Rev.* **2002**, *102*, 231–282.
(12) Pyykkö, P. *Angew. Chem., Int. Ed.* **2004**, *43*, 4412–4456.
(13) Wu, X.; Qin, Z.; Xie, H.; Wu, X.; Cong, R.; Tang, Z. *Chin. J. Chem. Phys.* **2010**, *23*, 373–380.
(14) Eppink, A.; Parker, D. H. *Rev. Sci. Instrum.* **1997**, *68*, 3477–3484.
(15) Dribinski, V.; Ossadtchi, A.; Mandelshtam, V. A.; Reisler, H. *Rev. Sci. Instrum.* **2002**, *73*, 2634–2642.
(16) (a) Becke, A. D. *Phys. Rev. A* **1988**, *38*, 3098–3100. (b) Lee, C.; Yang, W.; Parr, R. G. *Phys. Rev. B* **1988**, *37*, 785–789.
(17) Perdew, J. P.; Wang, Y. *Phys. Rev. B* **1992**, *45*, 13244–13249.
(18) Perdew, J. P.; Burke, K.; Ernzerhof, M. *Phys. Rev. Lett.* **1996**, *77*, 3865–3868.
(19) Perdew, J. P. *Phys. Rev. B* **1986**, *33*, 8822–8824.
(20) ADF2007.01; *SCM, Theoretical Chemistry*; Vrije Universiteit: Amsterdam, The Netherlands, 2007.
(21) Lenthe, E. v.; Baerends, E. J.; Snijders, J. G. *J. Chem. Phys.* **1993**, *99*, 4597–4610.
(22) (a) Ziegler, T.; Rauk, A. *Theor. Chem. Acc.* **1977**, *46*, 1–10. (b) Bickelhaupt, F. M.; Nibbering, N. M. M.; Van Wezenbeek, E. M.; Baerends, E. J. *J. Phys. Chem.* **1992**, *96*, 4864–4873.
(23) (a) Purvis, G. D.; Bartlett, R. J. *J. Chem. Phys.* **1982**, *76*, 1910. (b) Hampel, C.; Peterson, K. A.; Werner, H.-J. *Chem. Phys. Lett.* **1992**, *190*, 1. (c) Knowles, P. J.; Hampel, C.; Werner, H.-J. *J. Chem. Phys.* **1994**, *99*, 5219. (d) Deegan, M. J. O.; Knowles, P. J. *Chem. Phys. Lett.* **1994**, *227*, 321.
(24) Frisch, M. J.; Trucks, G. W.; Schlegel, H. B.; Scuseria, G. E.; Robb, M. A.; Cheeseman, J. R.; Montgomery, J. A., Jr.; Vreven, T.;

Kudin, K. N.; Burant, J. C.; Millam, J. M.; Iyengar, S. S.; Tomasi, J.; Barone, V.; Mennucci, B.; Cossi, M.; Scalmani, G.; Rega, N.; Petersson, G. A.; Nakatsuji, H.; Hada, M.; Ehara, M.; Toyota, K.; Fukuda, R.; Hasegawa, J.; Ishida, M.; Nakajima, T.; Honda, Y.; Kitao, O.; Nakai, H.; Klene, M.; Li, X.; Knox, J. E.; Hratchian, H. P.; Cross, J. B.; Adamo, C.; Jaramillo, J.; Gomperts, R.; Stratmann, R. E.; Yazyev, O.; Austin, A. J.; Cammi, R.; Pomelli, C.; Ochterski, J. W.; Ayala, P. Y.; Morokuma, K.; Voth, G. A.; Salvador, P.; Dannenberg, J. J.; Zakrzewski, V. G.; Dapprich, S.; Daniels, A. D.; Strain, M. C.; Farkas, O.; Malick, D. K.; Rabuck, A. D.; Raghavachari, K.; Foresman, J. B.; Ortiz, J. V.; Cui, Q.; Baboul, A. G.; Clifford, S.; Cioslowski, J.; Stefanov, B. B.; Liu, G.; Liashenko, A.; Piskorz, P.; Komaromi, I.; Martin, R. L.; Fox, D. J.; Keith, T.; Al-Laham, M. A.; Peng, C. Y.; Nanayakkara, A.; Challacombe, M.; Gill, P. M. W.; Johnson, B.; Chen, W.; Wong, M. W.; Gonzalez, C.; Pople, J. A. *Gaussian 03*; Gaussian, Inc.: Wallingford, CT, 2004.

(25) (a) Andrae, D.; Häussermann, U.; Dolg, M.; Stoll, H.; Preuss, H. *Theor. Chim. Acta* **1990**, *77*, 123.(b) Dolg, M. Effective Core Potentials. In *Modern Methods and Algorithms of Quantum Chemistry*, Band 3, Proceedings 2, Auflage; Grotendorst, J., Ed.; NIC Series; John von Neumann Institute for Computing; Jülich, 2000; pp 507−540.

(26) (a) Ervin, K. M.; Ramond, T. M.; Davico, G. E.; Schwartz, R. L.; Casey, S. M.; Lineberger, W. C. *J. Phys. Chem. A* **2001**, *105*, 10822–10831.(b) Ervin, K. M. *PESCAL*, 2010, Fortran program.

(27) Evans, C. J.; Gerry, M. C. L. *J. Mol. Spectrosc.* **2000**, *203*, 105–117.

(28) Zare, R. N. *J. Chem. Phys.* **1964**, *40*, 1934–1944.

(29) Dietz, O.; Rayon, V. M.; Frenking, G. *Inorg. Chem.* **2003**, *42*, 4977–4984.

(30) Wang, X. B.; Wang, Y. L.; Yang, J.; Xing, X. P.; Li, J.; Wang, L. S. *J. Am. Chem. Soc.* **2009**, *131*, 16368–16370.